Cobalt-substituted porous calcium copper titanate electrodes for paracetamol degradation by an electro-oxidation/peroxymonosulfate system

Elissa Makhoul, Fida Tanos, Rebecca Manouguian, Maged F Bekheet, Wiebke Riedel, Eddy Petit, Geoffroy Lesage, Marc Cretin, Madona Boulos, David Cornu, et al.

Applied Surface Science 669 (2024) 160430

Contents lists available at ScienceDirect

Applied Surface Science

journal homepage: www.elsevier.com/locate/apsusc

Full Length Article

Cobalt-substituted porous calcium copper titanate electrodes for paracetamol degradation by an electro-oxidation/peroxymonosulfate system

Elissa Makhoul [a,b], Fida Tanos [a], Rebecca Manouguian [a], Maged F. Bekheet [c], Wiebke Riedel [d], Eddy Petit [a], Geoffroy Lesage [a], Marc Cretin [a], Madona Boulos [b], David Cornu [a], Mikhael Bechelany [a,e,*]

[a] Institut Européen des Membranes, IEM, UMR 5635, Univ Montpellier, ENSCM, Centre National de la Recherche Scientifique (CNRS), Place Eugène Bataillon, 34095 Montpellier, France
[b] Laboratoire de Chimie Physique des Matériaux (LCPM/PR2N), EDST, Université Libanaise, Faculté des Sciences II, Département de Chimie, Fanar, Lebanon
[c] Technische Universität Berlin, Faculty III Process Sciences, Institute of Materials Science and Technology, Chair of Advanced Ceramic Materials, Straße des 17. Juni 135, Berlin 10623, Germany
[d] Freie Universität Berlin, Institut für Chemie und Biochemie, Arnimallee 22, 14195 Berlin, Germany
[e] Gulf University for Science and Technology, GUST, Kuwait

ARTICLE INFO

Keywords:
Cobalt-substituted perovskite
$CaCu_{2.5}Co_{0.5}Ti_4O_{12}$
Cu/Co-peroxymonosulfate activation
Electrocatalysis
Paracetamol degradation

ABSTRACT

Developing cobalt-substituted perovskite electroactive membranes with an efficient Co/Cu combination mode is an important environmental challenge for removing drugs *via* peroxymonosulfate (PMS) activation. In this work, cobalt (Co)-substituted calcium copper titanatewas synthesized with an easy ball milling process and used as an anode in electro-oxidation in the presence of PMS for paracetamol degradation. The Co-CCTO anode with a Co ratio of 0.5 showed the highest removal efficiency (100 % of 10 ppm paracetamol after 180 min) due to the increase of the active sites and the appearance of the Co^{2+}/Co^{3+} cycle that accelerates the charge transfer with Co incorporation into the lattice. Scavenger experiments showed that sulfate radicals ($SO_4^{\cdot-}$), oxygen radicals ($O_2^{\cdot-}$), hydroxyl radicals (OH), and singlet oxygen ($^1O_2$) were generated in the electro-oxidation-PMS reaction system and that $SO_4^{\cdot-}$, $^1O_2$, and $O_2^{\cdot-}$ were the dominant active radicals. The toxicity tests with *Vibrio fischeri* confirmed paracetamol mineralization and decomposition and the elimination of harmful by-products. It is crucial to explore the substitution of CCTO with different metal dopants in order to optimize the membrane performance and overcome the limitations associated with cobalt substitution.

1. Introduction

Water pollution is caused mostly by the discharge of domestic and industrial effluent waste, leakage from water tanks, urbanization, marine dumping, radioactive waste, and atmospheric deposition. Inorganic (metal ions, oxyacid ions) and organic (organic dyes, pesticides and pharmaceutical compounds) substances in water are the main pollutants [1–4]. Pharmaceutical pollutants are now a major problem that increases the potential risk for human health and the environment. This can lead to biodiversity loss, alterations in wildlife behavior and contamination of the food chain, and also contributes to a variety of health issues, including antibiotic resistance, endocrine system alterations, and gastrointestinal infections [5–7]. Paracetamol is a widely consumed over-the-counter drug; however, its biodegradability is limited. Consequently, it may transform into different, more harmful metabolites, such as aminophenol and phenol, and might remain in the environment for extended periods [8–11].

In the context of these challenges, research is primarily focused on advancing and safeguarding potable water production. By addressing the shortcomings of traditional water treatment techniques, such as coagulation, flocculation, sedimentation or filtration, new approaches try to enhance the removal of contaminants, especially persistent

* Corresponding author at: Institut Européen des Membranes, IEM, UMR 5635, Univ Montpellier, ENSCM, Centre National de la Recherche Scientifique (CNRS), Place Eugène Bataillon, 34095 Montpellier, France.
E-mail address: mikhael.bechelany@umontpellier.fr (M. Bechelany).

https://doi.org/10.1016/j.apsusc.2024.160430
Received 17 March 2024; Received in revised form 21 May 2024; Accepted 30 May 2024
Available online 31 May 2024

pharmaceutical compounds. Current methods exhibit various limitations, such as variable efficiency against pharmaceuticals, the generation of hazardous by-products and the need of harmful chemicals [12–15]. Advanced oxidation processes offer improved efficiency, effectiveness, and sustainability for water treatment and purification. Particularly, electro-oxidation, which uses electric current, generates highly reactive oxidizing species that can break down organic and inorganic pollutants in wastewater. This technology shows promise for the treatment of wastewater containing pharmaceutical compounds and offers several advantages compared with other advanced oxidation processes. For instance, it is a more energy-efficient method compared to UV and ozone [16–18]. Moreover, it can remove a wide range of pollutants, including non-biodegradable and toxic pollutants, can operate at a wide range of pH values, and does not require the addition of chemicals [19–23].

In addition, the incorporation of sulfate radicals in conjunction with electro-oxidation offers multiple advantages. Sulfate radicals have a high oxidation potential, are non-selective in their reactivity, and have a relatively long lifespan in water, which allows them to continue reacting with pollutants even after the electro-oxidation process ends. Unlike other oxidants, such as chlorine, sulfate radicals do not produce harmful by-products that persist in the water or harm the environment. Overall, the use of sulfate radicals in electro-oxidation has several advantages that make it a promising technology for water treatment [24–27]. Different methods, such as thermal activation, metal-based activation and photoactivation, can be used to generate sulfate radicals from PMS activation.

Various composite types have been used as anodes for electrocatalysis with PMS activation. Perovskite materials have recently demonstrated their potential as catalysts for PMS activation in water treatment systems. Metal-oxide perovskites have a distinctive crystal structure and are well-suited for catalytic applications. Recently, many groups investigated perovskite-based catalysts due to their efficacy in PMS activation, leading to the degradation of organic pollutants [28]. For instance, Zhu *et al.* reported that 91.6 % of ibuprofen was degraded under light irradiation in 60 min through the activation of sulfate radicals by forming a Cu^{+}/Cu^{2+} redox couple using a $CaCu_3Ti_4O_{12}$ (CCTO) photocatalyst [29]. We previously demonstrated the effect of porous CCTO [30] and its treatment under different atmospheres [31] to enhance PMS activation. We found that the incorporation of 30 % of poly(methyl methacrylate) (PMMA) increased the percentage of the CuO phase, as well as the electrochemical properties, thereby enhancing PMS activation. Total paracetamol (PCM) degradation was achieved in 180 min. Thermal treatment resulted in CCTO decomposition into Cu, $CaTiO_3$, and Ti_9O_{17} phases upon exposure to hydrogen. After decomposition in the presence of hydrogen, PCM degradation was achieved in 10 min by electro-oxidation using PMS. This was attributed to the enhanced conductivity and electrochemical activity. Similarly, the A-site/B-site doping strategy improved PMS activation by perovskite by modifying the coordination environment and leading to more active sites [32,33]. Studies on cobalt (Co)-doped perovskite catalysts showed that they are the most efficient PMS activators. Zhang *et al.* found that atrazine degradation was increased using Co-doped $LaFeO_3$ and attributed this effect to a synergistic role of bimetallic rings [Fe(III)/Fe(II) and Co(III)/Co(II) rings] [34]. Moreover, Li *et al.* used Co-doped Ruddlesden-Popper perovskite for PMS activation and reported that 98 % of rhodamine B was removed in 30 min [35].

This work involved the use of Co-substituted CCTO (Co-CCTO) perovskite for water treatment. Specifically, it evaluated the effects of combining Co and Cu on PMS activation and PCM degradation. The present study focused on Co-CCTO perovskite in a combined system of electro-oxidation and PMS activation. The Co-CCTO perovskite membranes were synthesized by ball milling. Different Co ratios were investigated to optimize the properties for electrocatalytic degradation of PCM. Furthermore, the radicals responsible for the degradation and the acute ecotoxicity of the solution were studied.

2. Experimental section

2.1. Chemicals

PMMA (CAS Number: 9011-14-7), titanium (IV) oxide (TiO_2, 99.5 %, CAS Number: 13463-67-7), potassium chloride (KCl, ≥99.0 %, CAS Number: 7447-40-7), calcium carbonate ($CaCO_3$, 98 %, CAS Number: 471-34-1), poly(vinyl alcohol) (PVA, 99 %, CAS Number: 9002-89-5), copper (II) oxide (surface: CuO, bulk: Cu_2O, CAS Number: 1317-38-0), cobalt (II-III) oxide (Co_3O_4, CAS Number: 1308-06-1), potassium hydroxide (KOH, ≥85 %, CAS Number: 01900-20-08), sodium sulfate (Na_2SO_4, ≥99 %, CAS Number: 7757-82-6), p-benzoquinone ($C_6H_4O_2$, ≥99.5 %, CAS Number: 106-51-4), PMS (CAS Number: 70693-62-8), PCM (≥99 % CAS Number: 103-90-2), *tert*-butanol (TBA, $(CH_3)_3COH$, ≥99.5 %, CAS Number: 75-65-0), sodium chloride (NaCl, ≥99 %, CAS Number: 7647-14-5), and methanol (CH_3OH, ≥99.9 %, CAS Number: 67-56-1) were purchased from Sigma Aldrich. All chemicals were used without any further purification.

2.2. Preparation of CCTO porous membranes

To oxidize Cu_2O to CuO, the copper (II) oxide precursor was treated at 600 °C under air for 30 min. Co-CCTO (i.e., $CaCu_{3-x}Co_xTi_4O_{12}$) perovskites with different Co content (x = 0, 0.1, 0.5, 0.7, and 0.9) were obtained by mixing $CaCO_3$, CuO (treated), Co_3O_4, and TiO_2 as precursors in a planetary ball mill (PM200, Retsch) in a stoichiometric ratio. The resulting phase was calcined under air and mixed with PMMA in a ball mill using the conditions given in Table 1. The powder with 5 wt% PVA (binder) was pressed using a hydraulic press. The pellet (20 mm diameter and 1–2 mm thickness) was sintered in air (Table 1). Six pellets were prepared: bare CCTO without Co (CCTO), and CCTO-0.1, CCTO-0.5, CCTO-0.7, and CCTO-0.9 with Co contents of x = 0, 0.1, 0.5, 0.7, and 0.9, respectively.

2.3. Structural characterization

The microstructure, morphology, crystallinity, and phase composition of the different CCTO samples were examined by scanning electron microscopy (SEM; Hitachi S4800), energy dispersive X-ray analysis (EDX), raman spectroscopy (Horiba XploRA) using a 659.55 nm laser, and X-ray diffraction (XRD) using Cu-Kα radiation (λ = 1.5406 Å), the FULLPROF software and profile function 7. The chemical elemental composition and oxidation states were determined by X-ray photoelectron spectroscopy (XPS; ESCALAB 250 spectrometer). Paramagnetic species in the catalysts were assessed by electron paramagnetic resonance (EPR) measurements. Inductively coupled plasma mass spectrometry (ICP-MS) (Thermo Scientific®, iCAP TQ) was used to measure ion leaching.

2.4. Electrochemical properties

The charge transport resistance was examined with impedance spectrometry (EIS). For this test, a three-electrode system (CCTO is working electrode, Ag/AgCl is reference electrode, and platinum wire is

Table 1
Experimental conditions for the preparation of CCTO with different Co ratios (x = 0; 0.1, 0.5, 0.7 and 0.9).

Step	Speed	Hours
Ball milling of precursor	350 rpm	5
Calcination	5°/900 °C	3
Ball milling with PMMA	250 rpm	1
Sintering	2°/240 °C → 1°/420 °C → 2°/850 °C → 5°/1100 °C	3

counter electrode) was used in a Solartron SI 1287 potentiostat/galvanostat with frequency from 0.01 Hz to 105 MHz and voltage bias of 10 mV amplitude. The electrolyte (1 M KOH) was degassed with pure argon for 30 min before each test to eliminate oxygen.

2.5. PCM degradation

The electro-oxidation activity of CCTO/Co-CCTO membranes was evaluated by monitoring PCM degradation. The experimental conditions are listed in Table 2.

At specific reaction times, a 2 mL aliquot was taken and PCM concentration was measured by liquid chromatography coupled to tandem mass spectrometry according to [36]. To verify the membrane recyclability, PCM degradation was evaluated for five cycles in the same conditions.

Eq. (1) shows how PCM degradation efficiency was calculated [37]:

$$Removalefficiency(\%) = \frac{(C_0 - C)}{C_0} \bullet 100 \quad (1)$$

where C_0 (mg/L), and C (mg/L) are the initial PCM concentration and PCM concentration in the solution at different time points, respectively.

2.6. Scavenger studies

To identify the main active radical species involved in the electro-oxidation system during PCM mineralization, scavenger tests were performed. Benzoquinone for superoxide ($O_2^{\bullet-}$), L-histidine for oxygen radicals and singlet oxygen ($^1O_2$), TBA for hydroxyl ($^{\bullet}OH$), and methanol for sulfate ($SO_4^{\bullet-}$) and $^{\bullet}OH$ radicals were added to the solution at 6.6, 6.6, 660 and 660 mM, respectively. The experimental conditions used in these tests were the same as those for PCM degradation.

2.7. Acute toxicity tests and total organic carbon

Vibrio fischeri LCK 487 and a TOC-L CSH/CSN Shimadzu analyzer (Japan) were used for the toxicity tests to assess the acute toxicity and Total Organic Carbon (TOC) removal, respectively, of the solution aliquots collected during PCM degradation by electro-oxidation, as previously described [30].

3. Results and discussion

3.1. Characterization of the synthesized composites

The membrane morphology and composition were examined using SEM/EDX measurements (Fig. 1). The CCTO membrane displayed a composite morphology with large grains that contained significant amounts of Ca and Ti and grain boundaries that were enriched in Cu. The O element was distributed on the whole surface. The morphology remained almost unchanged in Co-CCTO membranes where x was ≤ 0.7. In these membranes, Co was incorporated into the large Ca- and Ti-containing grains (Fig. S1-2). Conversely, morphology was different in the CCTO-0.9 membrane with the highest Co ratio. This might be related to cobalt distribution on the surface, suggesting the decomposition of the CCTO phase and the formation of Co_2TiO_4, as revealed by the XRD analysis (Fig. 2).

The XRD analysis showed that the pure CCTO sample (Fig. 2**a**) was composed of CCTO as the main phase (93.3 ± 0.9 wt%) with a minor impurity phase of CuO (6.7 ± 0.5 wt%). CuO is usually observed as a precipitate phase at the grain boundaries of sintered CCTO materials [30,31]. In the CCTO-0.5 sample, the weight fraction of the CuO phase slightly increased to 7.6 ± 0.5 wt%, and no Co-related crystalline phase was observed in the XRD pattern (Fig. 2**b and d**). Moreover, the lattice parameter of the cubic CCTO phase in the CCTO-05 sample increased from 7.4039(1) Å to 7.4048(1) Å (Fig. 2**e**). In the CCTO-0.9 sample (Fig. 2**c**), the lattice parameter of CCTO increased to 7.4073(1) Å, the weight fraction of CuO remarkably decreased to 1.5 ± 0.1 wt%, and 1.6 ± 0.1 wt% of Co_2TiO_4 phase was formed. The increase in the lattice parameter of the CCTO phase with the increasing Co concentration (Fig. 2**e**) suggests the substitution of larger Co^{2+} by smaller Ti^{4+} cations in the cubic structure [r (Co^{2+}, high spin) = 0.745 Å, r (Ti^{4+}) = 0.605 Å; all cations are 6-fold coordinated] [38]. The ionic size of Co^{3+} in a high spin state and 6-fold coordination is ~0.61 Å [38], which is quite similar to that of Ti^{4+}. Similarly, the ionic size of Co^{2+} in 4-fold coordination is ~0.58 Å, which is very close to that of Cu^{2+} cations (0.57 Å) in the same coordination [38]. Although the last two substitutions are not expected to increase significantly the lattice parameter of the CCTO phase, this cannot be excluded. The increase in the weight fraction of CuO impurity in the CCTO-0.5 sample suggests the substitution of both Cu^{2+} and Ti^{4+} by Co^{2+} in the CCTO lattice. However, with higher Co content ($x = 0.9$), not all Co cations can be included in the CCTO lattice, forming Co_2TiO_4 with Co^{2+} cations as impurity phase. Consequently, Ti^{4+} cation segregation in the CCTO lattice to form the Co_2TiO_4 phase results in stabilizing more Cu^{2+} cations in the CCTO lattice; thus, the weight fraction of the CuO phase is decreased in the CCTO-0.9 sample.

The continuous-wave EPR spectra normalized to the sample mass (Fig. 3**a**) exhibit a rather broad signal ($\Delta B_{pp} \approx 4$ mT) at $g \approx 2.15$, which was previously attributed to Cu^{2+} species in CCTO [30,31]. Although the linewidth and g-value of this signal were similar for all samples, the intensity strongly decreased with increasing Co content. The comparable linewidth observed for the different samples suggests comparable spin interactions of these Cu^{2+} species in all samples, but a lower number of these Cu^{2+} species in samples with higher Co content. Next to this signal, a broader signal ($\Delta B_{pp} > 80$ mT, $g \approx 2.2$) also was detected. The intensity and linewidth of this broader signal decreased with increasing Co content, consistent with a lower number of EPR-active species and lower spin interactions. This signal might be attributed to another type of Cu^{2+} species in CCTO in a different chemical environment [39]. In the literature, intensity and linewidth changes were reported after doping and also after CCTO reduction [39,40]. Moreover, these studies provided evidence for complex spin interactions of the EPR-active species. The observed changes upon Co addition clearly demonstrate its effect on magnetic species in CCTO. First, the difference in its effect on the spin interactions indicates the heterogeneity of the EPR-active species in the samples. Second, the number of all EPR-active species were lowered. This decrease could be caused by the formation of EPR-silent species, such as Cu^{+}, but also by delocalized spins.

Raman spectrometry analysis with a low intensity red laser was used to detect intra- and inter-molecular vibrations (Fig. 3**b**). In the CCTO sample, two strong bands at 445 cm^{-1} and 512 cm^{-1}, which characterize [TiO_6], were observed. As they are the main bands of CCTO, their finding confirmed CCTO formation in our sample, which is in agreement with the XRD results. In addition, a small band at 291 cm^{-1} (CuO mode) was detected [41]. Co introduction induced weak shifts in the position of the peak at 291 cm^{-1} that progressively increased with higher Co concentrations.

XPS analysis was used to determine the surface chemical states of all samples. The high-resolution XPS spectra were fitted using a Gaussian function and the detailed fitting parameters of Cu $2p_{3/2}$, Ti $2p_{3/2}$ and

Table 2
Experimental conditions for monitoring PCM degradation using an electro-oxidation process with PMS activation by CCTO, CCTO-0.1, CCTO-0.5, CCTO-0.7 and CCTO-0.9.

Volume	210 mL (Milli Q water)
Initial PCM concentration	10 ppm
PMS concentration (active substance)	0.5 mM
Na_2SO_4 (electrolyte)	50 mM
Three-electrode system	Cathode: platinum Anode: $CCTO_{(x)}$ (2 cm)Reference electrode: Ag/AgCl

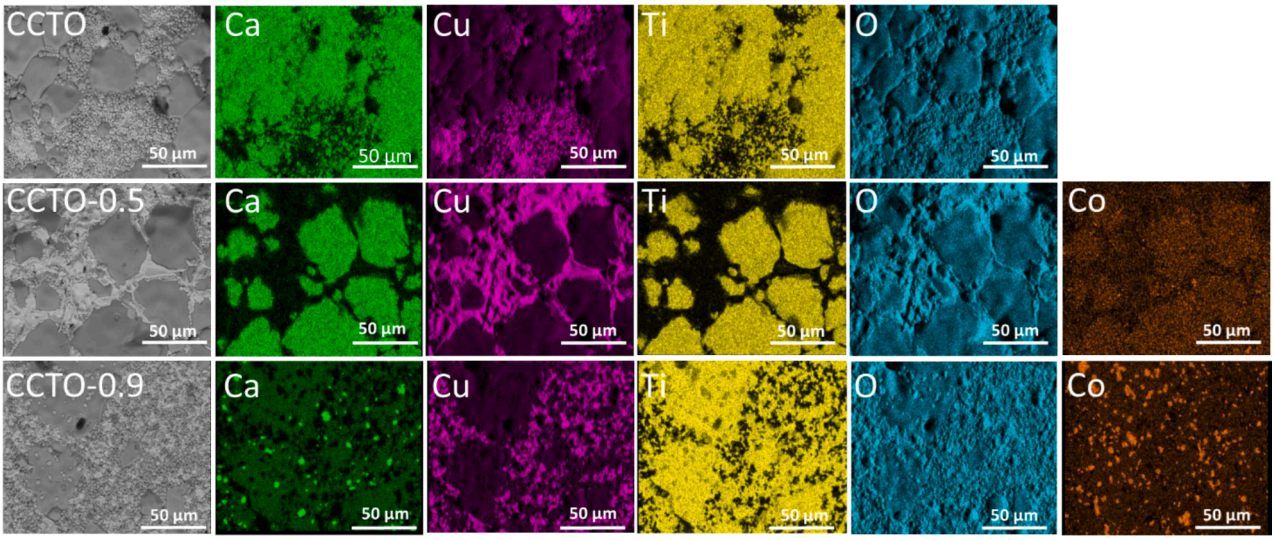

Fig. 1. SEM/EDX mapping of the CCTO membranes with different cobalt ratios (x = 0; 0.5, and 0.9).

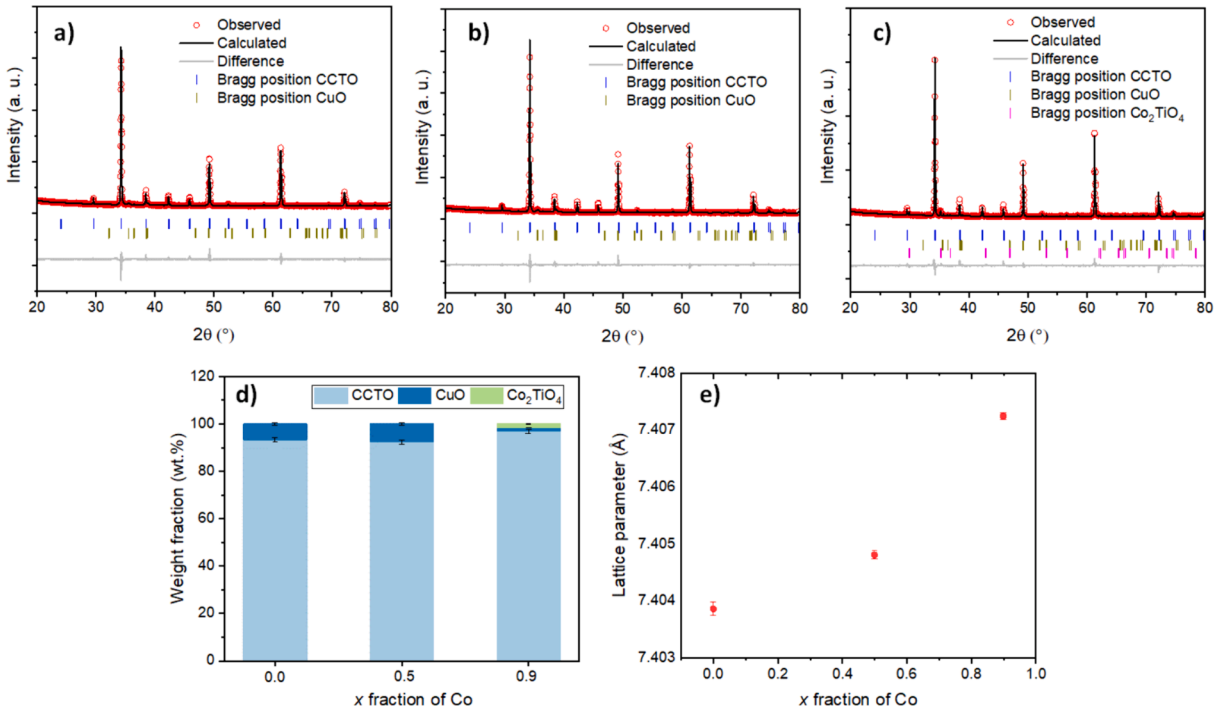

Fig. 2. Structure refinement of powder XRD data collected at room temperature for unsubstituted CCTO (a), and Co-substituted CCTO with x = 0.5 (b) and x = 0.9 (c), showing the observed (red circle) and calculated (black solid line) intensities, the calculated Bragg reflections (tick marks), and the difference (grey solid line). (d) Weight fractions of the formed crystalline phases and (e) Lattice parameter of the CCTO phase extracted by Rietveld refinement of the ex situ powder XRD patterns in function of the mole fraction of Co substitution.

O1s are listed in Table 3. In the CCTO membrane, the results showed the presence of Cu and Ti in the 2+ and 4+ oxidation states, respectively [42,43]. The O 1s spectra were deconvoluted into two peaks at 529.7 eV (assigned to the Cu–O or Ti–O bonding), and at 531.6 eV (surface adsorbed oxygen O–H) [44,45]. Upon Co addition, the deconvolution of Cu $2p_{3/2}$ and Ti $2p_{3/2}$ led to the co-existence of Cu^{+}/Cu^{2+} and Ti^{3+}/Ti^{4+} [46] (Table 3). Fig. 3**c** shows the high-resolution Co 2p spectra with the Co $2p_{3/2}$ (779.9 eV) and Co $2p_{1/2}$ (796.9 eV) peaks observed in CCTO-0.5 and CCTO-0.9. After deconvolution, the Cu $2p_{3/2}$ and Cu $2p_{1/2}$ peaks were composed of two peaks. The two peaks at 778.1 eV and 796.1 eV were attributed to Co^{2+}, and the two peaks at 981.8 and 797.3 eV to Co^{3+}. The presence of mixed valence states, i.e. Co^{2+}/Co^{3+}, Cu^{+}/Cu^{2+} and Ti^{3+}/Ti^{4+}, indicates Co incorporation [46–48]. The deconvolution of the O 1s signals detected in CCTO-0.5 and CCTO-0.9 (Fig. 2**d**) highlighted the appearance of a peak at 530.4 eV that was assigned to Co-O bonds. This confirmed the substitution by Co and the formation of Co_2TiO_4, as shown by XRD.

The physicochemical data indicated the formation of the CCTO phase in the region of large grains, while the CuO impurity phase was present in the grain boundary regions. The impurity phase was due to the eutectic point of Cu that leads to a liquid phase at high temperatures [49]. Following Co substitution (x = 0.5), cobalt was introduced in the large grains, increasing the percentage of CuO from 6.7 % to 7.6 %. With higher Co amounts (x = 0.9), the excess of Co led to the formation of

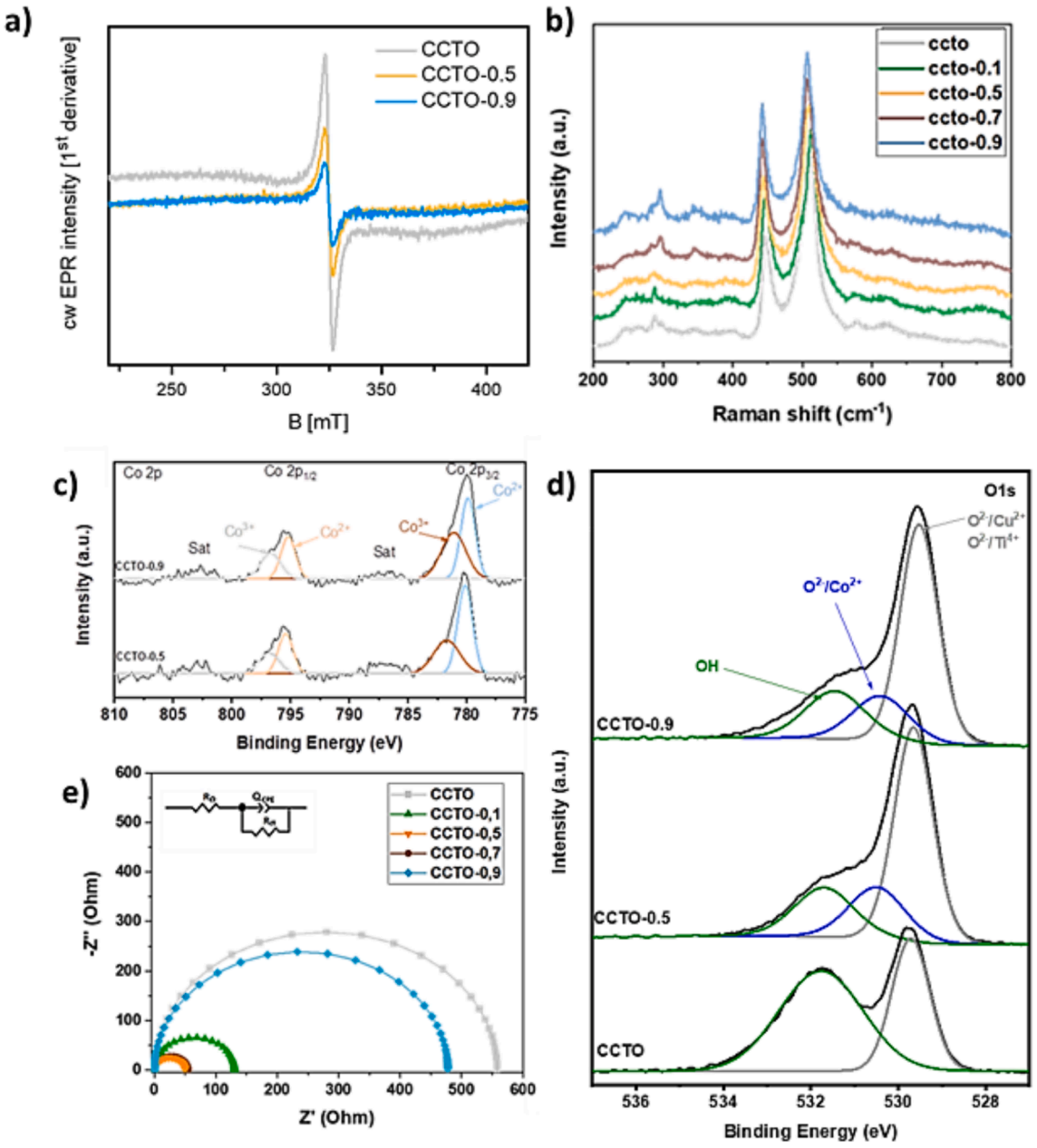

Fig. 3. (a) Room temperature cw EPR spectra of ccto, ccto-0.5 and ccto-0.9 normalized to sample mass; (b) Raman shifts of CCTO samples with different Co ratios (x = 0; 0.1; 0.5; 0.7 and 0.9); (c) High-resolution XPS spectra of Co2p in CCTO-0.5 and CCTO-0.9; (d) High-resolution XPS spectra of O1s in CCTO, CCTO-0.5 and CCTO-0.9; and (e) EIS data for all samples.

Table 3
XPS fitting parameters of the Cu 2p, Ti 2p and O 1s signals.

	CCTO	CCTO-0.5	CCTO-0.9
Cu^{2+} $2p_{3/2}$	934.1	933.9	933.6
Cu^{1+} $2p_{3/2}$	–	932.6	932.2
Ti^{4+} $2p_{3/2}$	458.7	458.1	458.1
Ti^{3+} $2p_{3/2}$		458.58	458.52
O 1s OH	531.6	531.7	531.5
O 1s O2-A (A = Cu or Ti)	529.7	529.6	529.5
O 1s O2_B (B = Co)	–	530.5	530.4

Co_2TiO_4, the decrease of the CCTO phase and the incorporation of Co^{2+} into Ti^{4+}, as shown by the XRD data, and resulted in Co dispersion all over the membrane.

Then, a three-electrode system in 1 M KOH was used to determine the charge transfer and activity of the CCTO membranes. In the Nyquist plots of the EIS measurements (Fig. 3**e**), the high radius of the semicircle for CCTO indicated that it exhibited the highest charge transfer electrical resistance among the samples under study [50–52]. In the Co-CCTO samples, the arc radius decreased, indicative of a lower charge transfer resistance, confirming the acceleration of the electron transfer upon Co addition (Fig. 3**e**) [35]. A comparison of the resistance values showed that CCTO-0.5 had the lowest resistance, indicating that it displays the fastest interfacial charge migration. This could be due to the high percentage of CuO, as calculated by Rietveld refinement, and the presence of the Co mixed-valence states confirmed by XPS [53,54].

3.2. *Electro-oxidation activity*

The electro-oxidation activity of the CCTO membranes with different Co content (x = 0, 0.1, 0.5, 0.7, and 0.9) was evaluated by monitoring

PCM degradation by electro-oxidation *via* PMS activation. The Co-free CCTO electrode exhibited the lowest degradation efficiency: only 76 % of PCM was degraded after 180 min of operation (Fig. 4**a**). Efficiency improved by increasing the Co content in the membranes: 100 % of PCM was degraded in the presence of the CCTO-0.5 anode after 180 min. This improvement may be linked to the elevated CuO percentage, determined by Rietveld refinement, and the existence of mixed-valence states of Co (XPS data). Moreover, CCTO-0.5 exhibited the lowest resistance, improving charge transfer. This electrode showed the highest current and electron conductivity, as verified by chronoamperometry (Fig. S3). Additionally, Co incorporation and the increasing of the CuO phase appeared to generate more active sites, making of CCTO-0.5 a promising catalyst for PMS activation. Both Co^{3+} and Cu^{2+} lead to PMS decomposition, resulting in the generation of the sulfate radicals $SO_5^{\cdot-}$ and $SO_4^{\cdot-}$ (Eqs. 2–5) [34,55]. However, these slow reactions are limiting for PMS activation. To overcome this limitation, electro-oxidation was used to promote Co^{2+}/Cu^{1+} regeneration, PMS activation and oxygen and sulfate radical formation (Eqs. 6–9). In addition, the electrochemical potential of Co^{3+}/Co^{2+} is higher than that of Cu^{2+}/Cu^{+} (1.81 V vs 0.17 V) and this facilitates the formation of Cu^{2+} and Co^{2+} (Eq. 10) [56,57].

The generated oxygen and hydroxyl radicals can be the main pathway for $^1O_2$ generation (Eq. 11) [56,58]. The formation of oxygen, hydroxyl and sulfate radicals may induce PCM decomposition into by-products that will be mineralized into CO_2 and water (Eq. 12).

$$Cu^{2+} + HSO_5^- \rightarrow Cu^{1+} + SO_4^{\cdot-} + OH^- \quad (2)$$

$$Co^{3+} + HSO_5^- \rightarrow Co^{2+} + SO_4^{\cdot-} + OH^- \quad (3)$$

$$Cu^{1+} + HSO_5^- \rightarrow Cu^{2+} + SO_5^{\cdot-} + H^+ \quad (4)$$

$$Co^{2+} + HSO_5^- \rightarrow Co^{3+} + SO_5^{\cdot-} + H^+ \quad (5)$$

$$HSO_5^- + e^- \rightarrow SO_4^{\cdot-} + OH^- \quad (6)$$

$$e^- + O_2 \rightarrow O_2^{\cdot-} \quad (7)$$

$$HSO_5^- + e^- \rightarrow SO_4^{\cdot-} + OH^- \quad (8)$$

$$Co^{3+}/Cu^{2+} + e^- \rightarrow Cu^{1+} / Co^{2+} \quad (9)$$

$$Co^{3+} + Cu^{+} \rightarrow Co^{2+} + Cu^{2+} \quad (10)$$

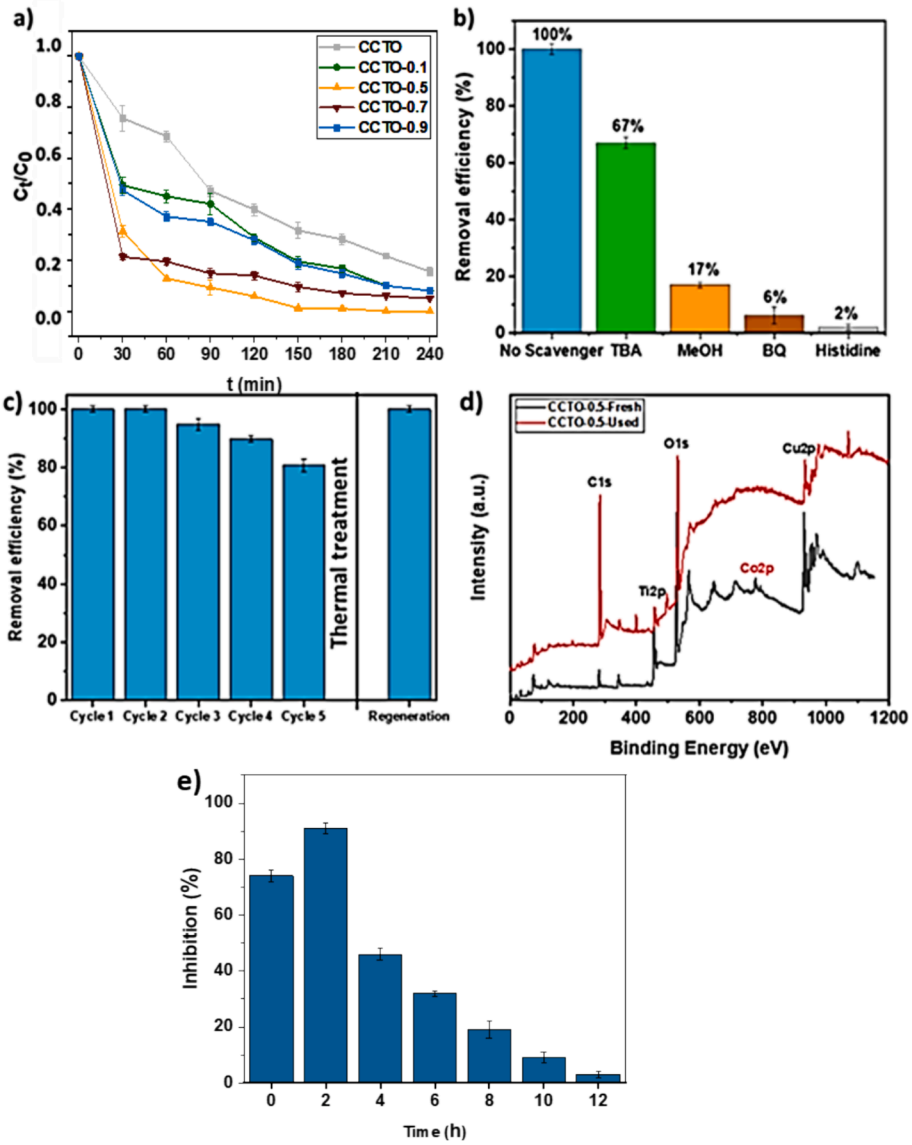

Fig. 4. (a) PCM degradation by electro-oxidation; (b) radical scavenger test; (c) CCTO-0.5 stability over five successive cycles; (d) XPS spectrum of CCTO-0.5 before and after PCM degradation; (e) toxicity test based on *V. fischeri* luminescence inhibition. Conditions: [PCM] = 10 ppm, [PMS] = 0.5 mM, [TBA] = 660 mM, [methanol] = 660 mM, [p-benzoquinone] = 6.6 mM, and [L-histidine] = 6.6 mM; each experiment was repeated three times.

$O_2^{\cdot-} + {}^{\cdot}OH \rightarrow {}^1O_2 + OH^-$(11)

ROS + PCM → by-products → $CO_2 + H_2O$(12)

A scavenger test was then used to identify the main radicals implicated in PCM degradation. This test was performed in the same conditions used for monitoring PCM degradation (10 ppm PCM, 0.5 mM PMS, and 50 mM Na_2SO_4) with the addition or not of the scavengers (TBA, L-histidine, p-benzoquinone, and methanol). TBA, which inhibits OH radicals [59,60], decreased PCM removal efficiency from 100 % to 67 %. Methanol, which inhibits OH and sulfate radicals [61], further decreased PCM degradation to 17 %. Addition of p-benzoquinone [62] and L-histidine, which inhibits oxygen radicals and singlet oxygen ($^1O_2$) respectively, hindered electro-oxidation and resulted in the degradation of only 7 % and 2 % of PCM (Fig. 4**b**). In conclusion, singlet oxygen, oxygen, and sulfate radicals are mainly responsible for PCM degradation by electro-oxidation *via* PMS activation, while OH plays only a minor role.

The stability of the CCTO-0.5 anode was studied by monitoring PCM degradation over five cycles. PCM degradation remained stable after two cycles (Fig. 4**c**), and then decreased to 95.9 % (third cycle), 84.7 % (fourth cycle) and 80.7 % (fifth cycle). The 20 % decrease after five cycles may be due to Co release or the accumulation of the product in the membrane pores, which reduces the number of active sites [59,63]. To understand this decrease in activity, XPS, XRD, SEM analyses and ICP-MS were performed to evaluate the transformation of the used electrode. No difference was observed in the morphology and XRD diffraction patterns after five cycles of degradation (Fig. S4). The XPS survey of the CCTO-0.5 electrode before and after PCM degradation (Fig. 4**d**) showed the disappearance of the Co2p peaks in the used CCTO-0.5 sample, which was due to Co release (1.67 ppb) in the solution. Therefore, to promote Co diffusion from the bulk of larger Co-containing grains to their surface, the used CCTO-0.5 membrane was treated at 1100 °C for 3 h and then used for PCM degradation in the usual conditions. The membrane efficiency was fully restored as indicated by the complete PCM degradation in 180 min (Fig. 4**c**).

A toxicity test using *V. fischeri* was carried out to determine the acute toxicity of the solution [64]. The interaction of *V. fischeri* with the PCM solution (50 mM Na_2SO_4, 0.5 mM PMS, and 10 ppm PCM) led to 74 % of inhibition of the luminescence signal. After 2 h of electro-oxidation, inhibition of the luminescence signal was increased to 92 % due to the generation of by-products that are more harmful than PCM, such as 1,4-benzoquinone, benzoic acid, and benzaldehyde, as demonstrated by previous works [64–66]. These by-products were then transformed into non-toxic compounds, such as carboxylic acids, as indicated by the decrease of luminescence inhibition to 46 % after 4 h, to 19 % after 8 h, and to 3 % after 12 h (Fig. 4**e**) [65,67].

Additionally, the results obtained from the TOC analysis during PCM degradation provided valuable insights. A significant 38 % reduction in TOC was observed in the first 4 h of the experiment. This percentage remained stable even after 8 h, which can be attributed to the formation of short aliphatic chains (e.g. fumaric, oxalic, acetic, and maleic acids) through the ongoing chemical processes. Noteworthy, despite TOC conversion into these shorter aliphatic compounds, toxicity was not increased, as indicated by the toxicity test.

According to the literature [63,64,68], PCM degradation is likely to involve the creation of three intermediate compounds: 4-aminophenol, acetamide, and N-(3,4-dihydroxyphenyl) formamide. These intermediates are formed by breaking bonds due to the attack of free radicals on aromatic rings and acetyl-amino groups. N-(3,4-dihydroxyphenyl) formamide reacts with ·OH to produce benzoic acid and acetamide, which then leads to formic acid and acetic acid. Additionally, reactive radicals targeting the aromatic rings linked to 4-aminophenol can generate hydroquinone. When oxidized by free radicals, hydroquinone yields short-chain organic acids, such as carboxylic acid. All these by-products are converted into CO_2, H_2O, and inorganic ions at the end of the degradation process.

Co-substituted perovskite materials have attracted much interest in recent years for many applications, specifically as extremely active anodes for wastewater treatment *via* electrocatalytic oxidation. Co-CCTO samples have been tested in recent studies for improving CCTO dielectric, nonlinear, and magnetic properties [46,69,70], and for increasing the electrical response [71,72]. However, the electro-oxidation activity of Co-CCTO membranes for water remediation has never studied before. Therefore, their electro-oxidation activity was compared to that of other perovskite materials (Table 4). This comparison showed that the CCTO-0.5 membrane is an interesting new strategy to increase the efficiency of advanced oxidation for organic wastewater treatment, with minimal current use.

4. Conclusion

In this study, we investigated Co influence for improving PCM degradation by electro-oxidation. Various Co-CCTO membranes ($CaCu_{3-x}Co_xTi_4O_{12}$, x = 0, 0.1, 0.5, 0.7, and 0.9) were synthesized using ball milling. When x was <0.7, cobalt was incorporated in the CCTO lattice, leading to an increase in the CuO phase from 6.7 % to 7.6 %. A higher cobalt amount (x = 0.9) resulted in the formation of Co_2TiO_4. The presence of Co accelerated electron transfer. These improvements led to the complete degradation of PCM (10 ppm) by electro-oxidation (1.5 V) *via* activation of PMS (0.5 mM) using CCTO-0.5 as anode in 180 min. The $SO_4^{\cdot-}$, $O_2^{\cdot-}$ radicals and $^1O_2$ played significant roles in PCM degradation, while •OH radicals contributed to a lesser extent. The CCTO-0.5 anode stability was assessed over five cycles of PCM degradation. The 20 % decrease after five cycles could be attributed to Co release or product accumulation in the membrane pores that reduces the number of active sites. XPS and ICP-MS revealed the disappearance of the Co 2p peaks and Co release at 1.67 ppb, respectively. Regenerating the CCTO-0.5 sample at 1100 °C for 3 h restored its degradation efficiency, as indicated by the complete degradation of PCM in 180 min. This suggested Co replenishment at the membrane surface. In addition, PCM mineralization and decomposition and the generation of harmful by-products were confirmed with a toxicity test. Therefore, Co-CCTO electrodes are a promising strategy to generate electrocatalytic materials to be used for the removal of persistent organic pollutants from wastewater by electro-oxidation *via* PMS activation. After verifying the capacity of Co-CCTO for the degradation of paracetamol, it is necessary to study its efficiency in wastewater, including different parameters such as pH and current density.

CRediT authorship contribution statement

Elissa Makhoul: Writing – original draft, Visualization, Validation, Methodology, Investigation, Formal analysis, Data curation, Conceptualization. **Fida Tanos:** Writing – original draft, Validation, Methodology, Investigation, Formal analysis, Data curation. **Rebecca Manouguian:** Writing – original draft, Validation, Methodology, Formal analysis, Data curation. **Maged F. Bekheet:** Writing – review & editing, Validation, Funding acquisition, Formal analysis, Conceptualization, Data curation. **Wiebke Riedel:** Writing – review & editing, Validation, Resources, Formal analysis, Data curation. **Eddy Petit:** Writing – review & editing, Validation, Investigation, Formal analysis, Data curation. **Geoffroy Lesage:** Writing – review & editing, Supervision, Methodology, Formal analysis, Data curation. **Marc Cretin:** Writing – review & editing, Supervision, Resources, Methodology, Conceptualization. **Madona Boulos:** Writing – review & editing, Validation, Supervision, Resources, Conceptualization. **David Cornu:** Writing – review & editing, Supervision, Resources, Investigation, Formal analysis. **Mikhael Bechelany:** Writing – review & editing, Visualization, Validation, Supervision, Project administration, Conceptualization.

Table 4
Comparison of studies on electrocatalytic degradation.

Pollutant	$C_{pollutant}$ (mg/L)	Anode material	Current or voltage	Solution volume (mL)	pH	Degradation time	Removal efficiency (%)	Ref.
Rhodamine B	100	$NiCo_2O_4$	10 mA/cm^2	50	7	60	97	[56]
Methyl red	140	Ti/CoTiO$_3$/Ce-PbO$_2$	30 mA/cm^2	100	7	180	90	[73]
4-chlorophenol	50	Ca-Mn-O	10 mA/cm^2	100	3	30	96	[74]
Methyl orange	20	Ti/$Sr_xLa_{1-x}MnyCo_{1-y}O_{3-\delta}$	20 mA/cm^2	200	9	60	99.61	[75]
Paracetamol	10	CCTO-0.5	1 mA/cm^2	210	7	180	100	This work

Declaration of competing interest

The authors declare that they have no known competing financial interests or personal relationships that could have appeared to influence the work reported in this paper.

Data availability

Data will be made available on request.

Acknowledgment

This study received partial support from Campus France through the PHC CEDRE project (49026ZJ).

Appendix A. Supplementary material

Supplementary data to this article can be found online at https://doi.org/10.1016/j.apsusc.2024.160430.

References

[1] Y. Liu, X. Chen, J. Zhao, W. Jin, K. Zhang, J. Qu, Y. Zhang, G. Chen, W.J.G. M. Peijnenburg, Development of a quantitative structure-activity relationship model for predicting quantum yield of hydroxyl radical generation from organic compounds, Environ. Sci.: Processes Impacts 25 (1) (2023) 66–74, https://doi.org/10.1039/D2EM00396A.

[2] L. Huang, X. Huang, J. Yan, Y. Liu, H. Jiang, H. Zhang, J. Tang, Q. Liu, Research progresses on the application of perovskite in adsorption and photocatalytic removal of water pollutants, J. Hazard. Mater. 442 (2023) 130024, https://doi.org/10.1016/j.jhazmat.2022.130024.

[3] Y. Wang, L. Li, X. Huang, Q. Li, G. Li, New insights into fluorinated TiO $_2$ (brookite, anatase and rutile) nanoparticles as efficient photocatalytic redox catalysts, RSC Adv. 5 (43) (2015) 34302–34313, https://doi.org/10.1039/C4RA17076H.

[4] M. Haseena, Water pollution and human, Health 1 (3) (2017) 4.

[5] B. Tiwari, B. Sellamuthu, Y. Ouarda, P. Drogui, R.D. Tyagi, G. Buelna, Review on fate and mechanism of removal of pharmaceutical pollutants from wastewater using biological approach, Bioresour. Technol. 224 (2017) 1–12, https://doi.org/10.1016/j.biortech.2016.11.042.

[6] K.H. Hama Aziz, Heterogeneous catalytic activation of peroxydisulfate toward degradation of pharmaceuticals diclofenac and ibuprofen using scrap printed circuit board, RSC Adv. 13 (1) (2023) 115–128, https://doi.org/10.1039/D2RA07263G.

[7] L.C. Aulsebrook, B.B.M. Wong, M.D. Hall, Can pharmaceutical pollution alter the spread of infectious disease? A case study using fluoxetine, Phil. Trans. R. Soc. B 2023 (378) (1873) 20220010, https://doi.org/10.1098/rstb.2022.0010.

[8] W.J. Lee, P.S. Goh, W.J. Lau, A.F. Ismail, Removal of pharmaceutical contaminants from aqueous medium: a state-of-the-art review based on paracetamol, Arab. J. Sci. Eng. 45 (9) (2020) 7109–7135, https://doi.org/10.1007/s13369-020-04446-1.

[9] R. Hernández, I. Olvera-Rodríguez, C. Guzmán, A. Medel, L. Escobar-Alarcón, E. Brillas, I. Sirés, K. Esquivel, Microwave-assisted sol-gel synthesis of an Au-TiO2 photoanode for the advanced oxidation of paracetamol as model pharmaceutical pollutant, Electrochem. Commun. 96 (2018) 42–46, https://doi.org/10.1016/j.elecom.2018.09.009.

[10] J.M.M. Henrique, M.K.S. Monteiro, J.C. Cardozo, C.A. Martínez-Huitle, D.R. Da Silva, E.V. Dos Santos, Integrated-electrochemical approaches powered by photovoltaic energy for detecting and treating paracetamol in water, J. Electroanal. Chem. 876 (2020) 114734, https://doi.org/10.1016/j.jelechem.2020.114734.

[11] A. Macías-García, J. García-Sanz-Calcedo, J.P. Carrasco-Amador, R. Segura-Cruz, Adsorption of paracetamol in hospital wastewater through activated carbon filters, Sustainability 11 (9) (2019) 2672, https://doi.org/10.3390/su11092672.

[12] W.L. Ang, A.W. Mohammad, N. Hilal, C.P. Leo, A review on the applicability of integrated/hybrid membrane processes in water treatment and desalination plants, Desalination 363 (2015) 2–18, https://doi.org/10.1016/j.desal.2014.03.008.

[13] G. Crini, E. Lichtfouse, Advantages and disadvantages of techniques used for wastewater treatment, Environ. Chem. Lett. 17 (1) (2019) 145–155, https://doi.org/10.1007/s10311-018-0785-9.

[14] F. Tanos, A. Razzouk, G. Lesage, M. Cretin, M. Bechelany, A comprehensive review on modification of titanium dioxide-based catalysts in advanced oxidation processes for water treatment, ChemSusChem (2023) e202301139.

[15] L. Zhang, L. Ju, X. Li, A. Guli, C. Lyu, CoOOH with a highly negative CB band for visible-light-driven photocatalytic degradation of refractory organic pollutants in peroxymonosulfate system: enhanced performance and multi-path synergetic mechanisms, J. Hazard. Mater. 460 (2023) 132403, https://doi.org/10.1016/j.jhazmat.2023.132403.

[16] M.E. Ghaith, M.G. Abd El-Moghny, G.A. El-Nagar, H.H. Alalawy, M.E. El-Shakre, M.S. El-Deab, Tailor-designed binary Ni–Cu nano dendrites decorated 3D-carbon

felts for efficient glycerol electrooxidation, RSC Adv. 13 (2) (2023) 895–905, https://doi.org/10.1039/D2RA06853B.
[17] E.K. Maher, K.N. O'Malley, M.E. Dollhopf, B.K. Mayer, P.J. McNamara, Removal of estrogenic compounds from water via energy efficient sequential electrocoagulation-electrooxidation, Environ. Eng. Sci. 37 (2) (2020) 99–108, https://doi.org/10.1089/ees.2019.0335.
[18] G. Ren, R. Li, M. Zhao, Q. Hou, T. Rao, M. Zhou, X. Ma, Membrane electrodes for electrochemical advanced oxidation processes: preparation, self-cleaning mechanisms and prospects, Chem. Eng. J. 451 (2023) 138907, https://doi.org/10.1016/j.cej.2022.138907.
[19] C.A. Martínez-Huitle, S. Ferro, Electrochemical oxidation of organic pollutants for the wastewater treatment: direct and indirect processes, Chem. Soc. Rev. 35 (12) (2006) 1324–1340, https://doi.org/10.1039/B517632H.
[20] Ngela Anglada, A. Urtiaga, I. Ortiz, Contributions of electrochemical oxidation to waste-water treatment: fundamentals and review of applications, J. Chem. Technol. Biotechnol. 84 (12) (2009) 1747–1755, https://doi.org/10.1002/jctb.2214.
[21] M. Priyadarshini, I. Das, M.M. Ghangrekar, L. Blaney, Advanced oxidation processes: performance, advantages, and scale-up of emerging technologies, J. Environ. Manage. 316 (2022) 115295, https://doi.org/10.1016/j.jenvman.2022.115295.
[22] M.S. Ahmad, M.H. Ab Rahim, T.M. Alqahtani, T. Witoon, J.-W. Lim, C.K. Cheng, A review on advances in green treatment of glycerol waste with a focus on electro-oxidation pathway, Chemosphere 276 (2021) 130128, https://doi.org/10.1016/j.chemosphere.2021.130128.
[23] C. Lyu, L. Zhang, D. He, B. Su, Y. Lyu, Micrometer-sized NiOOH hierarchical spheres for enhanced degradation of sulfadiazine via synergistic adsorption and catalytic oxidation in peroxymonosulfate system, Chin. Chem. Lett. 33 (2) (2022) 930–934, https://doi.org/10.1016/j.cclet.2021.07.012.
[24] J. Xu, Y. Liu, D. Li, C. Zhang, X. Fu, Y. Zhang, P. Wang, J. Lu, S. Chen, L. Li, Electrochemical activation of peroxymonosulfate by 3D printed blue TiO2 nanotube arrays reactive electrochemical membrane for efficient degradation of acetaminophen, J. Environ. Chem. Eng. 11 (3) (2023) 109602, https://doi.org/10.1016/j.jece.2023.109602.
[25] K. Zhao, Y. Zhang, Co 3 O 4 /carbon felt three-dimensional electrode promoted electrocatalytic oxidation – peroxymonosulfate system for p -nitrophenol degradation: effect of radical and non-radical mechanisms, J. Chem. Tech. Biotech. 98 (4) (2023) 940–948, https://doi.org/10.1002/jctb.7300.
[26] G. Zhang, S. Hu, X. Zhu, X. Hu, F. Yang, Electro-activation of peroxymonosulfate by β-PbO2 partial filling/covering TiO2 nanotube arrays anode for alkaloid berberine degradation: performance, mechanism and practicability, Chem. Eng. J. 457 (2023) 141009, https://doi.org/10.1016/j.cej.2022.141009.
[27] Y. Chen, X. Jiao, M. Du, R. Li, Y. Wei, Y. Zhang, Electrochemically promoted oxidation of oxytetracycline on MnO2@(PSS/PDDA)Au anode with peroxymonosulfate: mechanism and toxicity study, J. Taiwan Inst. Chem. Eng. 144 (2023) 104720, https://doi.org/10.1016/j.jtice.2023.104720.
[28] E. Makhoul, M. Boulos, M. Cretin, G. Lesage, P. Miele, D. Cornu, M. Bechelany, CaCu3Ti4O12 perovskite materials for advanced oxidation processes for water treatment, Nanomaterials 13 (14) (2023) 2119, https://doi.org/10.3390/nano13142119.
[29] Y. Zhu, T. Wang, W. Wang, S. Chen, E. Lichtfouse, C. Cheng, J. Zhao, Y. Li, C. Wang, CaCu3Ti4O12, an efficient catalyst for ibuprofen removal by activation of peroxymonosulfate under visible-light irradiation, Environ. Chem. Lett. 17 (1) (2019) 481–486, https://doi.org/10.1007/s10311-018-0776-x.
[30] E. Makhoul, F. Tanos, M.F. Bekheet, W. Riedel, E. Petit, R. Viter, I. Tepliakova, A. Ramanavicius, A. Razzouk, G. Lesage, M. Cretin, M. Boulos, D. Cornu, M. Bechelany, Porous calcium copper titanate electrodes for paracetamol degradation by electro-oxidation *via* CuO-induced peroxymonosulfate activation, Environ. Sci.: Nano (2023), https://doi.org/10.1039/D3EN00317E.
[31] E. Makhoul, F. Tanos, M.F. Bekheet, W. Riedel, E. Petit, G. Lesage, M. Cretin, M. Boulos, D. Cornu, M. Bechelany, A novel Magnéli-Phase Ti9O17-containing anode by controlled reductive decomposition of calcium copper titanate perovskite under hydrogen atmosphere for paracetamol degradation, Appl. Mater. Today 35 (2023) 101983, https://doi.org/10.1016/j.apmt.2023.101983.
[32] Y. Zhao, B. Huang, H. An, G. Dong, J. Feng, T. Wei, Y. Ren, J. Ma, Enhanced activation of peroxymonosulfate by Sr-doped LaFeO3 perovskite for orange i degradation in the water, Sep. Purif. Technol. 256 (2021) 117838, https://doi.org/10.1016/j.seppur.2020.117838.
[33] Y. Rao, Y. Zhang, J. Fan, G. Wei, D. Wang, F. Han, Y. Huang, J.-P. Croué, Enhanced peroxymonosulfate activation by Cu-doped LaFeO3 with rich oxygen vacancies: compound-specific mechanisms, Chem. Eng. J. 435 (2022) 134882, https://doi.org/10.1016/j.cej.2022.134882.
[34] H. Zhang, R. Zhang, Z. Wu, F. Yang, M. Luo, G. Yao, Z. Ao, B. Lai, Cobalt-doped boosted the peroxymonosulfate activation performance of LaFeO3 perovskite for atrazine degradation, Chem. Eng. J. 452 (2023) 139427, https://doi.org/10.1016/j.cej.2022.139427.
[35] Y. Li, Y. Wang, L. Liu, L. Tian, Oxygen-vacancy abundant electrospun co-doped ruddlesden-popper perovskite catalysts for peroxymonosulfate activation and rhodamine B degradation, J. Clean. Prod. 380 (2022) 135117, https://doi.org/10.1016/j.jclepro.2022.135117.
[36] S. Sayegh, M. Abid, F. Tanos, M. Cretin, G. Lesage, F. Zaviska, E. Petit, B. Navarra, I. Iatsunskyi, E. Coy, R. Viter, V. Fedorenko, A. Ramanavicius, A. Razzouk, J. Stephan, M. Bechelany, N-doped TiO2 nanotubes synthesized by atomic layer deposition for acetaminophen degradation, Colloids Surf. A Physicochem. Eng. Asp 655 (2022) 130213, https://doi.org/10.1016/j.colsurfa.2022.130213.
[37] M. Hosseini, A. Esrafili, M. Farzadkia, M. Kermani, M. Gholami, Degradation of ciprofloxacin antibiotic using photo-electrocatalyst process of Ni-doped ZnO deposited by RF sputtering on FTO as an anode electrode from aquatic environments: synthesis, kinetics, and ecotoxicity study, Microchem. J. 154 (2020) 104663, https://doi.org/10.1016/j.microc.2020.104663.
[38] R.D. Hannon, Revised effective ionic radii and systematic studies of interatomie distances in halides and chaleogenides, Acta Cryst A32 (1976) 751.
[39] M.A. Pires, C. Israel, W. Iwamoto, R.R. Urbano, O. Agüero, I. Torriani, C. Rettori, P. G. Pagliuso, L. Walmsley, Z. Le, J.L. Cohn, S.B. Oseroff, Role of oxygen vacancies in the magnetic and dielectric properties of the high-dielectric-constant system CaCu 3 Ti 4 O 12: an electron-spin resonance study, Phys. Rev. B 73 (22) (2006) 224404, https://doi.org/10.1103/PhysRevB.73.224404.
[40] M.C. Mozzati, C.B. Azzoni, D. Capsoni, M. Bini, V. Massarotti, Electron paramagnetic resonance investigation of polycrystalline CaCu $_3$ Ti $_4$ O 12, J. Phys.: Condens. Matter 15 (43) (2003) 7365–7374, https://doi.org/10.1088/0953-8984/15/43/018.
[41] M. Balık, V. Bulut, I.Y. Erdogan, Optical, structural and phase transition properties of Cu2O, CuO and Cu2O/CuO: their photoelectrochemical sensor applications, Int. J. Hydrogen Energy 44 (34) (2019) 18744–18755, https://doi.org/10.1016/j.ijhydene.2018.08.159.
[42] S. Maity, M. Samanta, A. Sen, K.K. Chattopadhyay, Investigation of electrochemical performances of ceramic oxide CaCu3Ti4O12 nanostructures, J. Solid State Chem. 269 (2019) 600–607, https://doi.org/10.1016/j.jssc.2018.10.016.
[43] L.-T. Mei, H.-I. Hsiang, T.-T. Fang, Effect of copper-rich secondary phase at the grain boundaries on the varistor properties of CaCu $_3$ Ti $_4$ O 12 ceramics, J. Am. Ceram. Soc. 91 (11) (2008) 3735–3737, https://doi.org/10.1111/j.1551-2916.2008.02674.x.
[44] S. Kawrani, M. Boulos, M.F. Bekheet, R. Viter, A.A. Nada, W. Riedel, S. Roualdes, D. Cornu, M. Bechelany, Segregation of copper oxide on calcium copper titanate surface induced by graphene oxide for water splitting applications, Appl. Surf. Sci. 516 (2020) 146051, https://doi.org/10.1016/j.apsusc.2020.146051.
[45] S. Kawrani, A.A. Nada, M.F. Bekheet, M. Boulos, R. Viter, S. Roualdes, P. Miele, D. Cornu, M. Bechelany, Enhancement of calcium copper titanium oxide photoelectrochemical performance using boron nitride nanosheets, Chem. Eng. J. 389 (2020) 124326, https://doi.org/10.1016/j.cej.2020.124326.
[46] J. Wang, Z. Lu, T. Deng, C. Zhong, Z. Chen, Improved dielectric, nonlinear and magnetic properties of cobalt-doped CaCu3Ti4O12 ceramics, J. Eur. Ceram. Soc. 38 (10) (2018) 3505–3511, https://doi.org/10.1016/j.jeurceramsoc.2018.04.015.
[47] N. Zhuk, E. Ipatova, B. Makeev, S. Nekipelov, A. Koroleva, L. Koksharova, R. Korolev, Spectroscopic study of Co-doped CaCu3Ti4O12, Lett. Mater. 11 (4) (2021) 386–391, https://doi.org/10.22226/2410-3535-2021-4-386-391.
[48] Z. Xu, Y. Wu, X. Wang, Q. Ji, T. Li, H. He, H. Song, S. Yang, S. Li, S. Yan, L. Zhang, Z. Zou, Identifying the role of oxygen vacancy on cobalt-based perovskites towards peroxymonosulfate activation for efficient iohexol degradation, Appl Catal B 319 (2022) 121901, https://doi.org/10.1016/j.apcatb.2022.121901.
[49] J. Li, M.A. Subramanian, H.D. Rosenfeld, C.Y. Jones, B.H. Toby, A.W. Sleight, Clues to the giant dielectric constant of CaCu $_3$ Ti $_4$ O 12 in the defect structure of "SrC$_u$ 3 T$_i$ $_4$ O 12", Chem. Mater. 16 (25) (2004) 5223–5225, https://doi.org/10.1021/cm048345u.
[50] B.O. Orimolade, B.A. Koiki, G.M. Peleyeju, O.A. Arotiba, Visible light driven photoelectrocatalysis on a FTO/BiVO4/BiOI anode for water treatment involving emerging pharmaceutical pollutants, Electrochim. Acta 307 (2019) 285–292, https://doi.org/10.1016/j.electacta.2019.03.217.
[51] J. Zhong, J. Huang, Y. Liu, D. Li, C. Tan, P. Chen, H. Liu, X. Zheng, C. Wen, W. Lv, G. Liu, Construction of double-functionalized g-C3N4 heterojunction structure via optimized charge transfer for the synergistically enhanced photocatalytic degradation of sulfonamides and H2O2 production, J. Hazard. Mater. 422 (2022) 126868, https://doi.org/10.1016/j.jhazmat.2021.126868.
[52] G. Huang, W. Ye, C. Lv, D.S. Butenko, C. Yang, G. Zhang, P. Lu, Y. Xu, S. Zhang, H. Wang, Y. Zhu, D. Yang, Hierarchical red phosphorus incorporated TiO2 hollow sphere heterojunctions toward superior photocatalytic hydrogen production, J. Mater. Sci. Technol. 108 (2022) 18–25, https://doi.org/10.1016/j.jmst.2021.09.026.
[53] T. Haq ul, Haik, Y.S. Doped, Cu2O-CuO nanoneedles array: free standing oxygen evolution electrode with high efficiency and corrosion resistance for seawater splitting, Catal. Today 400–401 (2022) 14–25, https://doi.org/10.1016/j.cattod.2021.09.015.
[54] J.R. Petrie, H. Jeen, S.C. Barron, T.L. Meyer, H.N. Lee, Enhancing perovskite electrocatalysis through strain tuning of the oxygen deficiency, J. Am. Chem. Soc. 138 (23) (2016) 7252–7255, https://doi.org/10.1021/jacs.6b03520.
[55] Q. Zeng, J. Tan, B. Gao, T. Cai, Q. Zhang, Y.-L. Liu, S. Chang, S. Zhao, S. Wu, Embedding Co in perovskite MoO3 for superior catalytic oxidation of refractory organic pollutants with peroxymonosulfate, Chemosphere 314 (2023) 137726, https://doi.org/10.1016/j.chemosphere.2022.137726.
[56] J. Di, M. Zhu, R. Jamakanga, X. Gai, Y. Li, R. Yang, Electrochemical activation combined with advanced oxidation on NiCo2O4 nanoarray electrode for decomposition of rhodamine B, J. Water Process Eng. 37 (2020) 101386, https://doi.org/10.1016/j.jwpe.2020.101386.
[57] F. Ghanbari, J. Wu, M. Khatebasreh, D. Ding, K.-Y.-A. Lin, Efficient treatment for landfill leachate through sequential electrocoagulation, electrooxidation and PMS/UV/CuFe2O4 process, Sep. Purif. Technol. 242 (2020) 116828, https://doi.org/10.1016/j.seppur.2020.116828.
[58] X. Pang, Y. Guo, Y. Zhang, B. Xu, F. Qi, LaCoO3 perovskite oxide activation of peroxymonosulfate for aqueous 2-phenyl-5-sulfobenzimidazole degradation: effect of synthetic method and the reaction mechanism, Chem. Eng. J. 304 (2016) 897–907, https://doi.org/10.1016/j.cej.2016.07.027.

[59] M. Abid, E. Makhoul, F. Tanos, I. Iatsunskyi, E. Coy, G. Lesage, M. Cretin, D. Cornu, B.H. Amara, M. Bechelany, N-doped HNT/TiO2 nanocomposite by electrospinning for acetaminophen degradation, Membranes 13 (2) (2023) 204, https://doi.org/10.3390/membranes13020204.

[60] S. Sayegh, F. Tanos, A. Nada, G. Lesage, F. Zaviska, E. Petit, V. Rouessac, I. Iatsunskyi, E. Coy, R. Viter, D. Damberga, M. Weber, A. Razzouk, J. Stephan, M. Bechelany, Tunable TiO $_2$ –BN–Pd nanofibers by combining electrospinning and atomic layer deposition to enhance photodegradation of acetaminophen, Dalton Trans. 51 (7) (2022) 2674–2695, https://doi.org/10.1039/D1DT03715C.

[61] Y. Huang, J. Li, P. Du, X. Lu, Rational design of copper encapsulated within nitrogen-doped carbon core-shell nanosphere for efficiently photocatalytic peroxymonosulfate activation, J. Colloid Interface Sci. 597 (2021) 206–214, https://doi.org/10.1016/j.jcis.2021.04.016.

[62] M. Abid, S. Sayegh, I. Iatsunskyi, E. Coy, G. Lesage, A. Ramanavicius, B.H. Amara, A. Bechelany, M. Design of halloysite-based nanocomposites by electrospinning for water treatment, Colloids Surf. A Physicochem. Eng. Asp 651 (2022) 129696, https://doi.org/10.1016/j.colsurfa.2022.129696.

[63] M. Noorisepehr, B. Kakavandi, A.A. Isari, F. Ghanbari, E. Dehghanifard, N. Ghomi, F. Kamrani, Sulfate radical-based oxidative degradation of acetaminophen over an efficient hybrid system: peroxydisulfate decomposed by ferroferric oxide nanocatalyst anchored on activated carbon and UV light, Sep. Purif. Technol. 250 (2020) 116950, https://doi.org/10.1016/j.seppur.2020.116950.

[64] T.X.H. Le, T.V. Nguyen, Z. Amadou Yacouba, L. Zoungrana, F. Avril, D.L. Nguyen, E. Petit, J. Mendret, V. Bonniol, M. Bechelany, S. Lacour, G. Lesage, M. Cretin, Correlation between degradation pathway and toxicity of acetaminophen and its by-products by using the electro-Fenton process in aqueous media, Chemosphere 172 (2017) 1–9, https://doi.org/10.1016/j.chemosphere.2016.12.060.

[65] M.D.G. de Luna, M.L. Veciana, C.-C. Su, M.-C. Lu, Acetaminophen degradation by electro-Fenton and photoelectro-Fenton using a double cathode electrochemical cell, J. Hazard. Mater. 217–218 (2012) 200–207, https://doi.org/10.1016/j.jhazmat.2012.03.018.

[66] H. Olvera-Vargas, J.-C. Rouch, C. Coetsier, M. Cretin, C. Causserand, Dynamic cross-flow electro-Fenton process coupled to anodic oxidation for wastewater treatment: application to the degradation of acetaminophen, Sep. Purif. Technol. 203 (2018) 143–151, https://doi.org/10.1016/j.seppur.2018.03.063.

[67] H.N. Phong Vo, G.K. Le, T.M. Hong Nguyen, X.-T. Bui, K.H. Nguyen, E.R. Rene, T. D.H. Vo, N.-D. Thanh Cao, R. Mohan, Acetaminophen micropollutant: historical and current occurrences, toxicity, removal strategies and transformation pathways in different environments, Chemosphere 236 (2019) 124391, https://doi.org/10.1016/j.chemosphere.2019.124391.

[68] Y. Zhang, Q. Zhang, J. Hong, Sulfate radical degradation of acetaminophen by novel iron-copper bimetallic oxidation catalyzed by persulfate: mechanism and degradation pathways, Appl. Surf. Sci. 422 (2017) 443–451, https://doi.org/10.1016/j.apsusc.2017.05.224.

[69] C. Mu, Y. Song, H. Wang, X. Wang, Room temperature magnetic and dielectric properties of cobalt doped CaCu $_3$ Ti $_4$ O 12 ceramics, J. Appl. Phys. 117 (17) (2015) 17B723, https://doi.org/10.1063/1.4916116.

[70] K.D. Mandal, A.K. Rai, L. Singh, O. Parkash, Dielectric properties of CaCu 2·9 Co 0·1 Ti 4 O 12 and CaCu 3 Ti 3·9 Co 0·1 O 12 ceramics synthesized by semi-wet route, Bull Mater Sci 35 (3) (2012) 433–438, https://doi.org/10.1007/s12034-012-0301-y.

[71] D. Xu, X. Yue, Y. Zhang, J. Song, X. Chen, S. Zhong, J. Ma, L. Ba, L. Zhang, S. Du, Enhanced dielectric properties and electrical responses of cobalt-doped CaCu3Ti4O12 thin films, J. Alloy. Compd. 773 (2019) 853–859, https://doi.org/10.1016/j.jallcom.2018.09.340.

[72] N.A. Zhuk, N.A. Sekushin, D.V. Sivkov, A.V. Popov, Electrical properties of Co-Doped CaCu3Ti4O12, Ceram. Int. 49 (2) (2023) 2486–2494, https://doi.org/10.1016/j.ceramint.2022.09.223.

[73] G. Dong, K. Lang, Y. Gao, W. Zhang, D. Guo, J. Li, D.-F. Chai, L. Jing, Z. Zhang, Y. Wang, A novel composite anode via immobilizing of Ce-doped PbO2 on CoTiO3 for efficiently electrocatalytic degradation of dye, J. Colloid Interface Sci. 608 (2022) 2921–2931, https://doi.org/10.1016/j.jcis.2021.11.023.

[74] T. Kong, Y. Wang, S. Liu, Y. Liu, M. Zhou, B. Li, X. Duan, C. Chen, S. Wang, Electron transfer to direct oxidation of aqueous organics by perovskites, Nano Res. (2023), https://doi.org/10.1007/s12274-023-5624-z.

[75] L. Chen, Y. Zhang, C. Ma, Perovskites SrxLa1-XMnyCo1-YO3-δ coated on Ti as stable non-noble anode for efficient electrocatalytic oxidation of organic wastewater containing ammonia nitrogen, Chem. Eng. J. 393 (2020) 124514, https://doi.org/10.1016/j.cej.2020.124514.